

**NLO QED contributions to top-pair production at hadron colliders**

W. Hollik and M. Kollár

*Max-Planck-Institut für Physik (Werner-Heisenberg-Institut), D-80805 München, Germany*

(Received 20 August 2007; published 8 January 2008)

Electroweak one-loop calculations for production of top-quark pairs at colliders are completed by providing the missing QED type contributions from real and virtual photons, where also effects from interference between QED and QCD contributions have to be taken into account. Moreover, photon-induced  $t\bar{t}$  production is included as another partonic channel.

DOI: [10.1103/PhysRevD.77.014008](https://doi.org/10.1103/PhysRevD.77.014008)

PACS numbers: 13.85.-t, 13.40.Ks, 13.85.Lg, 13.87.Ce

**I. INTRODUCTION**

Experimental investigations of the top quark at the Fermilab Tevatron have significantly contributed to precision tests of the standard model (SM) since the top discovery in 1995 [1,2]. The top quark mass is an important parameter within the SM and its precise knowledge is an essential ingredient to constrain the mass of the Higgs boson [3]. Besides the top mass, the measurement of the top-pair production cross section is an important test of the SM, and possible observation of deviations from the SM predictions could indicate new, nonstandard, contributions. Moreover, precise knowledge of the SM processes as a main source of background is crucial in direct searches for potential new physics beyond the SM.

At the Tevatron, the dominant production mechanism is the annihilation of quark-antiquark pairs  $q + \bar{q} \rightarrow t + \bar{t}$ , whereas at CERN LHC energies,  $t\bar{t}$  production proceeds mainly through gluon fusion,  $g + g \rightarrow t + \bar{t}$ . In lowest order, the  $t\bar{t}$  production cross section in hadronic collisions is of  $\mathcal{O}(\alpha_s^2)$  and was calculated in [4]. The corresponding lowest-order electroweak contributions of  $\mathcal{O}(\alpha^2)$  to the Drell-Yan annihilation process via  $\gamma$ - and  $Z$ -exchange are very small, contributing less than 1% at the partonic level [5], and are thus negligible. Accordingly, the main higher order contributions arise from QCD. Cross sections and distributions including QCD effects of  $\mathcal{O}(\alpha_s^3)$  were computed in [6,7], and an inspection of the QCD effects close to the production threshold was performed in [8]. Including the resummation of large logarithmic QCD contributions in the threshold region improves the perturbative calculation and was done in [9–13]. The predictions for the  $t\bar{t}$  production cross section currently used at the Tevatron are based on the studies in [14,15]. These include the next-to-leading-order (NLO) contributions with the resummation of soft logarithms (NLL) [14], and in addition, the next-to-next-to-leading-order (NNLO) soft-gluon corrections [15], extended to NNNLO in [16].

From the electroweak (EW) side, the EW one-loop corrections to the QCD-based lowest-order calculations, which are of  $\mathcal{O}(\alpha\alpha_s^2)$ , were investigated first in [17] for the subclass of the infrared-free nonphotonic contributions, i.e. those loop contributions without virtual photons. They are of special interest due to the large Yukawa coupling of the

top quark to the Higgs boson. However, they have little impact within the SM, about 1% of the lowest-order cross section for the Tevatron, and not more than 3% for the LHC [17,18]. In these calculations contributions including the interference of QCD and EW interactions were neglected. A study of the nonphotonic EW corrections with the gluon- $Z$  interference effects was done more recently in [19–22].

Still, a subset of the full EW corrections, corresponding to the QED corrections with real and virtual photons, was not included in the previous calculations. In this paper we close this gap and present the calculation of the missing QED subset, thus making the SM prediction at the one-loop level complete.

It is worth mentioning also several studies within specific extensions of the SM, comprising calculations of the Yukawa one-loop corrections within the general 2-Higgs-doublet model (G2HDM) for Tevatron [23] and LHC [24]. Also, the supersymmetric QCD (SUSY-QCD)  $\mathcal{O}(\alpha^2)$  contributions were calculated for Tevatron [25,26] and LHC [27], and for both [28]. The SUSY-EW corrections have been examined: partial calculations relevant for the Tevatron were done in [26], and a more complete description at  $\mathcal{O}(\alpha\alpha_s^2)$  within the G2HDM and the minimal supersymmetric standard model (MSSM) with numerical results for Tevatron and LHC, was presented in [29,30].

In the following, we provide the QED corrections to top pair production and also the effects arising from interference of QCD and QED interactions that occurs at one-loop order. Moreover, at this order the distribution of photons inside the proton has to be taken into account, adding photon-induced top production as another partonic channel at NLO. In the end, we present numerical results for both Tevatron and LHC.

Although our calculations are performed in the frame of the SM, they are also valid for extensions of the SM, as e.g. the MSSM and G2HDM.

**II. STRUCTURE OF THE QED CONTRIBUTIONS**

The QED contributions can be treated as a separate subclass at the electroweak one-loop level. They consist of virtual and real photon contributions, according to the topology of photonic insertions in the lowest-order graphs.

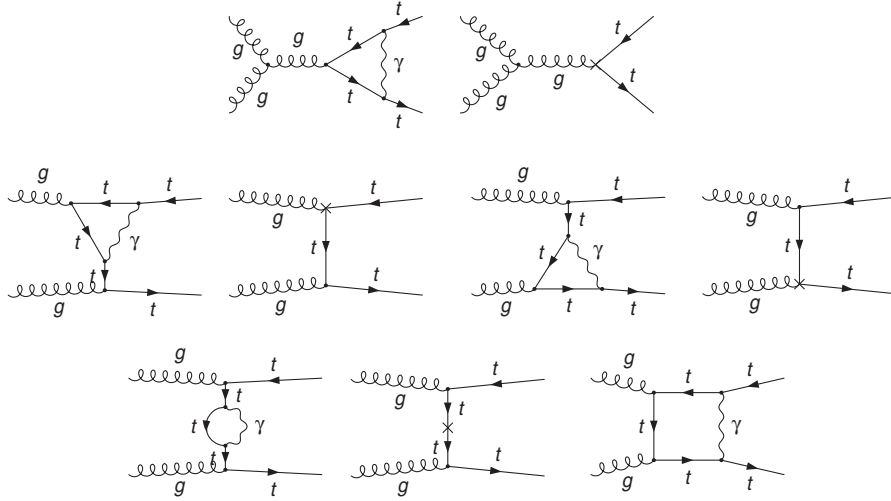


FIG. 1. Virtual QED  $\mathcal{O}(\alpha\alpha_s^2)$  contributions to gluon fusion ( $u$ -channel diagrams are not explicitly shown). Crossed lines and vertices denote counter term insertions.

Both real and virtual photon terms have to be combined in order to obtain a consistent, infrared (IR) finite result.

**A. Virtual corrections**

The virtual QED corrections consist of loop contributions with virtual photons. They can be described by the matrix elements  $\delta\mathcal{M}_a$ ,  $a = gg, q\bar{q}$ , for both partonic subprocesses separately. Contracting these quantities with the Born matrix elements  $\mathcal{M}_B^a$  yields the one-loop contribution to the differential cross sections at the partonic level of the order of  $\mathcal{O}(\alpha\alpha_s^2)$ , after spin and color summation,

$$\frac{d\hat{\sigma}_a^{(1\text{-loop})}}{d\hat{t}}(\hat{t}, \hat{s}) = \frac{1}{16\pi\hat{s}^2} \cdot 2 \operatorname{Re} \sum (\delta\mathcal{M}_a \cdot \mathcal{M}_B^{a*}), \quad (1)$$

where  $\hat{t}$  and  $\hat{s}$  are the usual Mandelstam variables. The explicit expressions of  $\mathcal{M}_B^a$  are given in [17], where the nonphotonic electroweak corrections have been studied. Throughout this paper we closely follow the notation of [17].

The virtual QED corrections of  $\mathcal{O}(\alpha\alpha_s^2)$ , contributing to  $\delta\mathcal{M}_a$ , can be classified according to self-energy, vertex, and box corrections, depicted by Feynman diagrams in

Figs. 1 and 2 for the two partonic processes of  $q\bar{q}$  annihilation and gluon fusion. They were treated with the help of the *FeynArts* [31], *FormCalc* [32], and *LoopTools* [33] packages, based on techniques from [34,35], which were further refined for 4-point integrals in [36,37]. The analytical expressions for the matrix elements are close to those in [17,38].

The whole set of QED loop diagrams is gauge invariant and UV-finite after taking into account the counter terms for the  $gq\bar{q}$ -vertex,  $gt\bar{t}$ -vertex and top quark self-energy. UV singularities in the sum of vertex functions and corresponding counter terms with quark field and mass renormalization constants cancel, hence, no coupling constant renormalization is needed.

To obtain finite vertices and propagators, it is thus sufficient to perform field and mass renormalization for the quarks. In the case of top quarks, the substitution

$$\Psi_t \rightarrow \left(1 + \frac{1}{2} \delta Z_t\right) \Psi_t, \quad m_t \rightarrow m_t - \delta m_t, \quad (2)$$

yields the counter term for the  $gt\bar{t}$ -vertex,  $\delta\Lambda_\mu$ , and for the top self-energy,  $\delta\Sigma$ , as follows:

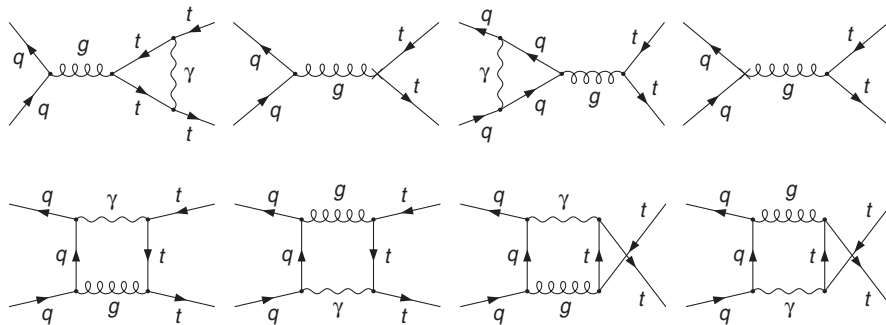
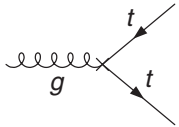
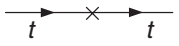


FIG. 2. Virtual QED  $\mathcal{O}(\alpha\alpha_s^2)$  contributions to  $q\bar{q}$  annihilation.



$$i\delta\Lambda_\mu = -ig_s T^c \gamma_\mu \delta Z_t, \quad (3)$$

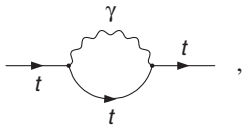


$$i\delta\Sigma = i(\not{p}\delta Z_t - m_t\delta Z_t + \delta m_t). \quad (4)$$

The field renormalization constant  $\delta Z_t$  as well as the mass counter term  $\delta m_t$  are fixed by renormalization conditions, for which we choose the on shell scheme. They are imposed on the renormalized top quark self-energy  $\hat{\Sigma} = \Sigma + \delta\Sigma$ , with

$$\Sigma(p) = \frac{\alpha}{4\pi} [\not{p}\Sigma_V(p^2) + m_t\Sigma_S(p^2)], \quad (5)$$

corresponding to the QED-like part of the unrenormalized top quark self-energy,



$$, \quad (6)$$

in the following way:

- (i) The pole of the top quark propagator is kept at  $m_t$  and thus defines the on shell mass:

$$\text{Re} \hat{\Sigma}(\not{p} = m_t) = 0, \quad \text{yielding} \quad (7)$$

$$\frac{\delta m_t}{m_t} = -(\Sigma_V + \Sigma_S)|_{p^2=m_t^2}.$$

- (ii) The residue of the top quark propagator is unity, yielding the field renormalization constant by (real parts only)

$$\delta Z_t = -\Sigma_V(m_t^2) - 2m_t^2 \frac{\partial}{\partial p^2} (\Sigma_V + \Sigma_S)|_{p^2=m_t^2}. \quad (8)$$

The renormalization constants for initial-state quarks ( $q$ ) are determined analogously, substituting  $m_t \rightarrow m_q$ . To obtain the counter terms for the initial state  $gq\bar{q}$  vertices, only the renormalization of the quark fields is necessary. Light quark masses are only kept where they are necessary to regularize collinear divergences, which appear as double logarithms  $\ln^2(\hat{s}/m_q^2)$  and single logarithms  $\ln(\hat{s}/m_q^2)$ .

As a consequence of the null photon mass, the virtual QED corrections are IR divergent. The photonic IR singularities can be regularized by introducing a fictitious photon mass  $\lambda$ .

A specific peculiarity of the QED corrections are the  $\mathcal{O}(\alpha\alpha_s)$  box contributions shown in Fig. 2, which contain besides photons also gluons in the loop. As a consequence, further IR singularities related to the gluons emerge from the loop integrals. Since the gluons appear quite similar to the photons in the box graphs, it is possible to perform the regularization by a gluon mass as well. For simplicity, we use the same regularization parameter  $\lambda$ .

### B. Real corrections

According to the Bloch-Nordsieck theorem [39], the IR singularities in the virtual corrections cancel against their counterparts from the real photon contributions after integration over the photon phase space. Therefore we have to include all contributions of the real photon radiation off the external particles to obtain an IR finite result. The corresponding diagrams are shown in Figs. 3 and 4.

Moreover, we have to include also gluon bremsstrahlung to compensate the IR singularities related to the gluons in the box graphs of Fig. 2. They consist of two types of diagrams: gluon radiation off the QED-mediated and off the QCD-mediated  $q\bar{q}$  annihilation, as depicted in Fig. 5.

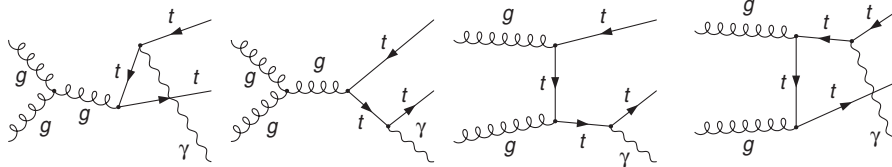


FIG. 3. Real QED  $\mathcal{O}(\alpha\alpha_s^2)$  contributions of photon bremsstrahlung to the  $gg$  fusion ( $u$ -channel diagrams are not explicitly shown).

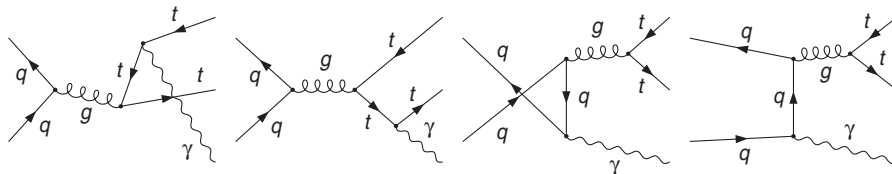


FIG. 4. Real QED  $\mathcal{O}(\alpha\alpha_s^2)$  contributions of photon bremsstrahlung to the  $q\bar{q}$  annihilation.

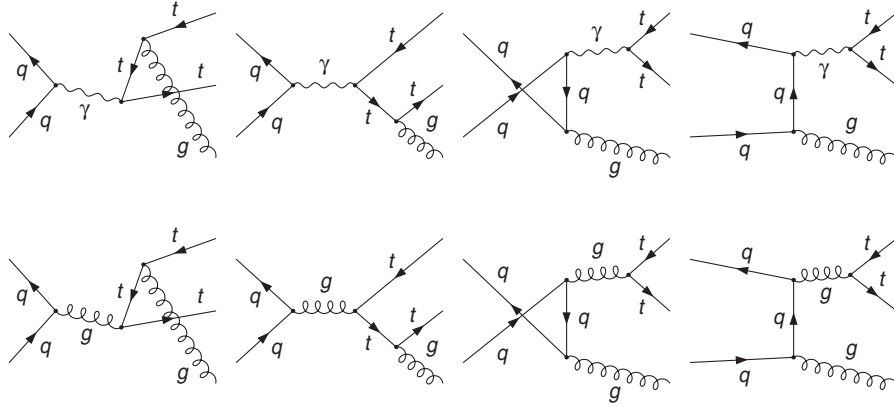


FIG. 5. Gluon bremsstrahlung from QED-mediated (upper row) and QCD-mediated (second row) Born diagrams, contributing at  $\mathcal{O}(\alpha\alpha_s^2)$  through interference.

At  $\mathcal{O}(\alpha\alpha_s^2)$ , it is the interference of these two classes of diagrams that is required, yielding a new type of QED–QCD interference. Still, not all of the interference terms contribute. Owing to the color structure, only the interference of the initial and final state gluon radiation graphs is nonzero, yielding the structure required to cancel the IR singular parts in the box corrections of Fig. 2. Nevertheless, the cancellation is not yet complete. The missing piece is the pure QCD box correction interfering with the QED  $q\bar{q}$  annihilation Born-level diagram, as displayed in Fig. 6, which gives another nonzero contribution of the same order. Only after combining all these various parts is the  $\mathcal{O}(\alpha\alpha_s^2)$  result IR finite.

In Fig. 6, only the photon-mediated Born-level diagram is shown. In principle, also the interference of the QCD box and Z-boson exchange tree-level diagram has to be taken into account. This contribution belongs to the IR singular gluon–Z corrections, which also contain the gluon–Z box graphs and gluon bremsstrahlung off Z-mediated tree-level diagrams. The IR singular structure of these contributions is simplified by the fact that there are no IR singularities related to the Z-boson. The gluon–Z interference effects were neglected in the original study of nonphotonic EW corrections performed in [17]. They have been investigated recently in [19–22].

For completeness of the NLO QED effects, photon radiation off the off shell top quarks in the  $gg$  fusion subprocess (Fig. 7) has to be considered as well. These effects are, however, 1 order of magnitude smaller than the

other terms and hence are less important for numerical studies.

Technically, for the phase space integration of real photon/gluon radiation, we apply the phase space slicing method (see appendix) taking advantage of its universality in handling both inclusive and noninclusive quantities. The dipole subtraction method [40], originally proposed for QCD [41], was used to verify numerical results obtained with the slicing method at the partonic level.

### C. Photon-induced $t\bar{t}$ production

In addition to the previously mentioned NLO QED contributions we also have to inspect the photon-induced production channels. These comprise at lowest order the gluon–photon fusion amplitudes illustrated in Fig. 8.

In general, photon-induced partonic processes vanish at the hadronic level unless the NLO QED effects are taken into account. A direct consequence of including these effects into the evolution of parton distribution functions (PDFs) is the nonzero photon density in the proton, which leads to photon-induced contributions at the hadronic level by convoluting the photon-induced partonic cross sections with the PDFs at NLO QED. Since the photon distribution function is of order  $\alpha$  they are formally not of the same overall order as the other NLO QED contributions. Numerically, however, they turn out to be sizeable, and we therefore include them in our discussion.

In view of a nontrivial interplay of formally different orders, we also mention that there are other contributions to  $t\bar{t}$  production of  $\mathcal{O}(\alpha_s\alpha^2)$ . These correspond to  $t\bar{t}$  pairs

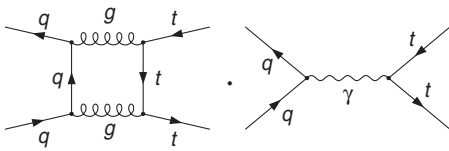


FIG. 6.  $\mathcal{O}(\alpha\alpha_s^2)$  contribution to  $q\bar{q}$  annihilation via QCD box diagrams (crossed diagram not explicitly shown) interfering with the QED Born diagram.

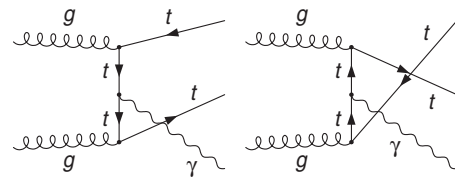


FIG. 7. IR-finite  $\mathcal{O}(\alpha\alpha_s^2)$  bremsstrahlung contributions.

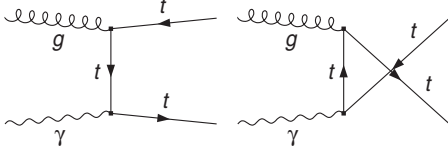


FIG. 8. Feynman diagrams for photon-induced  $t\bar{t}$  production at lowest order.

produced through an intermediate photon radiated off a light quark and can be attributed to the NLO QCD corrections to photon-mediated Drell-Yan top-pair production. As mentioned in Sec. I, those QED-like contributions are negligible with respect to the QCD channels, already at the Born level. They are 1 order of magnitude smaller than the QED corrections to the QCD-mediated Born terms considered here, as we checked explicitly by numerical evaluation. For this reason, we did not include them in our analysis.

Since the PDFs at NLO QED have become available only recently [42], the photon-induced hadronic processes have not yet been investigated. Here we present the first study of these effects on the top pair production.

### III. HADRONIC CROSS SECTION FOR $pp, p\bar{p} \rightarrow t\bar{t}X$

For obtaining the hadronic cross section we have to convolute the various partonic cross sections with the corresponding parton densities and sum over all contributing channels, adding up contributions of the nonradiative and radiative processes. As already mentioned, only the sum of all virtual and real corrections is IR finite. Final step is the factorization of the remaining mass singularities.

#### A. Mass factorization

The mass-singular logarithmic terms proportional to  $\ln(m_q)$  are not canceled in the sum of virtual and real corrections. They originate from collinear photon emission off the incoming light quarks. In analogy to the factorization of collinear gluon contributions, they have to be absorbed into the parton densities.

This can be formally achieved by replacing the bare quark distributions  $q_i(x)$  for each flavor by the appropriate scale dependent distributions  $q_i(x, Q^2)$  in the following way, according to [43] (with  $m_i = m_{q_i}$ ):

$$\begin{aligned}
 q_i(x, Q^2) = & q_i(x) + \frac{\alpha}{\pi} Q_i^2 q_i(x) \left\{ 1 - \ln \delta_s - \ln^2 \delta_s \right. \\
 & + \left( \ln \delta_s + \frac{3}{4} \right) \ln \left( \frac{Q^2}{m_i^2} \right) - \frac{1}{4} \lambda_{FC} f_{v+s} \left. \right\} \\
 & + \int_x^{1-\delta_s} \frac{dz}{z} q_i \left( \frac{x}{z} \right) \frac{\alpha}{2\pi} Q_i^2 \left\{ \frac{1+z^2}{1-z} \ln \left( \frac{Q^2}{m_i^2} \frac{1}{(1-z)^2} \right) \right. \\
 & \left. - \frac{1+z^2}{1-z} + \lambda_{FC} f_c \right\}, \quad (9)
 \end{aligned}$$

involving a soft-energy cut  $\delta_s$  and the functions

$$f_{v+s} = 9 + \frac{2\pi^2}{3} + 3 \ln \delta_s - 2 \ln^2 \delta_s, \quad (10)$$

$$f_c = \frac{1+z^2}{1-z} \ln \left( \frac{1-z}{z} \right) - \frac{3}{2(1-z)} + 2z + 3. \quad (11)$$

The expressions for the PDFs are given in both deep inelastic scattering (DIS) and modified minimal subtraction ( $\overline{\text{MS}}$ ) factorization schemes, which corresponds to  $\lambda_{FC} = 1$  and  $\lambda_{FC} = 0$ , respectively.

For a consistent treatment of the collinear singularities at  $\mathcal{O}(\alpha)$ , it is necessary to use an appropriate set of PDFs that was extracted from the data and evolved by Dokshitzer-Gribov-Lipatov-Altarelli-Parisi equations with the NLO QED effects included. Otherwise it would lead to an overestimation of the scale dependence. We use the PDFs from the MRST collaboration [42] which were determined at NLO QCD and NLO QED. The authors do not explicitly state which factorization scheme is relevant for NLO QED. We follow the reasoning given in [44] and use the DIS scheme in our calculation. For the numerical evaluation the factorization scale is set to  $Q = \mu_F = 2m_t$ . After performing the factorization of mass singularities, the results become free of the quark-mass logarithms. The scale dependence cannot be checked in a consistent way owing to the NLO QCD effects in the parton densities, as these are not included in our calculation. For this reason we do not present a study of the scale dependence.

#### B. Integrated hadronic cross sections

The observable hadronic cross section is obtained by convoluting the short distance partonic cross sections  $\hat{\sigma}_{gg}$ ,  $\hat{\sigma}_{q\bar{q}}$ ,  $\hat{\sigma}_{\gamma g}$  with the universal parton distribution functions for quarks, gluons, and photons. For colliding hadrons  $A$  and  $B$  carrying the momenta  $P_A$  and  $P_B$ , with  $S = (P_A + P_B)^2$ , the hadronic cross section can be expressed as

$$\begin{aligned}
 \sigma(S) = & \int_{(4m_t^2/S)}^1 d\tau \left[ \sum_i \mathcal{L}_{q_i \bar{q}_i}^{AB}(\tau) \hat{\sigma}_{q_i \bar{q}_i}(\hat{s}) + \mathcal{L}_{gg}^{AB}(\tau) \hat{\sigma}_{gg}(\hat{s}) \right. \\
 & \left. + \mathcal{L}_{\gamma g}^{AB}(\tau) \hat{\sigma}_{\gamma g}(\hat{s}) \right], \quad (12)
 \end{aligned}$$

with  $\tau = \hat{s}/S$ , and  $\hat{s}$  the partonic center-of-mass energy squared. The partonic cross sections  $\hat{\sigma}_{q\bar{q}}$  and  $\hat{\sigma}_{gg}(\hat{s})$  include the virtual photon and gluon loop contributions as well as the real photon and gluon bremsstrahlung terms, as described in Sec. II; the photon-induced partonic cross section  $\hat{\sigma}_{\gamma g}$  is of lowest order.



The parton luminosities are defined as follows:

$$\mathcal{L}_{mn}^{AB}(\tau) = \frac{1}{1 + \delta_{mn}} \int_{\tau}^1 \frac{dx}{x} \left[ \Phi_{m/A}(x, \mu_F) \Phi_{n/B}\left(\frac{\tau}{x}, \mu_F\right) + (1 \leftrightarrow 2) \right], \quad (13)$$

with the parton distributions inside  $A$ ,  $\Phi_{m/A} = q_i, g, \gamma$ , and the factorization scale,  $\mu_F$ .

### C. Differential hadronic cross sections

In addition to the integrated hadronic cross section it is convenient to define hadronic cross sections differential in one or more parameters. Typically, the variables are chosen to be Lorentz invariant quantities or quantities with simple transformation properties. In our study we consider the differential cross sections with respect to the invariant mass of the  $t\bar{t}$  pair (inclusive) and with respect to the transverse momentum of the top quark.

The invariant mass distribution of the hadronic cross section has the following form:

$$\frac{d\sigma}{d\sqrt{\hat{s}}} = \frac{2\sqrt{\hat{s}}}{S} \sum_{\{m,n\}} \mathcal{L}_{mn}^{AB}\left(\frac{\hat{s}}{S}\right) \hat{\sigma}_{mn}(\hat{s}), \quad (14)$$

where the sum extends over the various partons  $m, n$  in the initial state.

The differential hadronic cross section with respect to the transverse momentum of the top quark,  $p_T$ , can be written for the partonic  $2 \rightarrow 2$  processes as follows:

$$\frac{d\sigma}{dp_T} = \int_{\tilde{\tau}_0}^1 d\tau \mathcal{L}(\tau) \frac{\partial \hat{t}}{\partial p_T} \frac{d\hat{\sigma}}{d\hat{t}}(\hat{t}, \hat{s}) \quad (15)$$

(dropping parton indices and summation). The lower limit for the  $\tau$ -integration is thereby dependent on  $p_T$ ,

$$\tilde{\tau}_0 = \frac{4(m_t^2 + p_T^2)}{S}. \quad (16)$$

Real photonic/gluonic corrections belong to three-particle final states. Therefore, we also need the differential hadronic cross section with respect to the transverse momentum of the top quark, in each of the  $2 \rightarrow 3$  parton processes. Expressed in terms of variables of the parton center-of-mass system, it can be written in the following way:

$$\frac{d\sigma}{dp_T} = \int_{\tilde{\tau}_0}^1 d\tau \mathcal{L}(\tau) \int dk_1^0 \int dk_3^0 \int d\phi_3 \frac{\partial \cos\theta}{\partial p_T} \times \frac{d\hat{\sigma}}{dk_1^0 dk_3^0 d\phi_3 d\cos\theta}, \quad (17)$$

where  $k_1$  and  $k_3$  are the 4-momenta of the top quark and the photon(gluon).  $\theta$  is the angle between  $\vec{k}_1$  and the beam axis, given by  $\vec{P}_A$ , and  $\phi_3$  is the azimuthal angle of  $\vec{k}_3$  with respect to  $\vec{k}_1$  as polar axis. The threshold for the  $\tau$  integra-

tion corresponds to

$$\tilde{\tau}_0 S = \left( \sqrt{m_t^2 + p_T^2} + \sqrt{(m_t + \lambda)^2 + p_T^2} \right)^2, \quad (18)$$

with the IR mass regulator  $\lambda$ .

## IV. NUMERICAL RESULTS

In the following we present numerical results for the total hadronic cross section as well as for the distributions with respect to the invariant mass of the  $t\bar{t}$  pair and the transverse momentum of the top quark.

For the identification of  $t\bar{t}$  pairs and event reconstruction it is necessary to apply kinematical cuts, such as cuts to the transverse momentum and the pseudorapidity  $\eta$  of the  $t$  and  $\bar{t}$ . In the case of the LHC, the cuts applied are as follows:

$$p_T > 100 \text{ GeV} \quad \text{and} \quad |\eta| < 2.5. \quad (19)$$

For the Tevatron, the cuts are chosen according to

$$p_T > 25 \text{ GeV} \quad \text{and} \quad |\eta| < 2.5. \quad (20)$$

In Tables I and II, we present the numerical results for the integrated hadronic cross sections at the LHC and at the Tevatron, respectively. The values of  $\sigma$  are listed for the Born level and for the NLO QED corrections. The contri-

TABLE I. Integrated hadronic cross section for  $t\bar{t}$  production at the LHC, at NLO QED in different production subprocesses, without and with cuts.

Process	$\sigma_{\text{tot}}$ without cuts [pb]		$\sigma_{\text{tot}}$ with cuts [pb]	
	Born	Correction	Born	Correction
$u\bar{u}$	34.25	-1.41	18.64	-0.770
$d\bar{d}$	21.61	-0.228	11.54	-1.68
$s\bar{s}$	4.682	-0.0410	2.253	-0.0304
$c\bar{c}$	2.075	-0.0762	0.9630	-0.0446
$g\bar{g}$	407.8	2.08	213.6	0.524
$g\gamma$		4.45		2.29
$p\bar{p}$	470.4	4.78	247.0	1.80

TABLE II. Integrated hadronic cross section for  $t\bar{t}$  production at the Tevatron, at NLO QED in different production subprocesses, without and with cuts.

Process	$\sigma_{\text{tot}}$ without cuts [pb]		$\sigma_{\text{tot}}$ with cuts [pb]	
	Born	Correction	Born	Correction
$u\bar{u}$	3.411	-0.117	3.189	-0.118
$d\bar{d}$	0.5855	$-2.89 \times 10^{-3}$	0.5432	$-2.91 \times 10^{-3}$
$s\bar{s}$	$8.063 \times 10^{-3}$	$-1.21 \times 10^{-5}$	$7.343 \times 10^{-3}$	$-1.79 \times 10^{-5}$
$c\bar{c}$	$2.044 \times 10^{-3}$	$-5.06 \times 10^{-5}$	$1.857 \times 10^{-3}$	$-5.00 \times 10^{-5}$
$g\bar{g}$	0.4128	$3.17 \times 10^{-3}$	0.3803	$2.69 \times 10^{-3}$
$g\gamma$		0.0154		0.0143
$p\bar{p}$	4.420	-0.102	4.121	-0.104

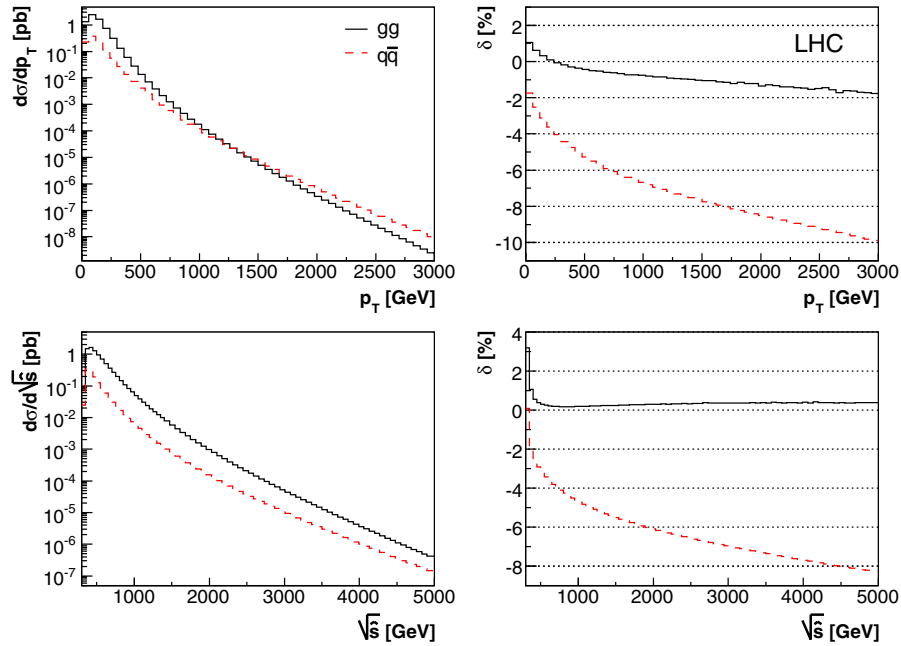


FIG. 9 (color online). Differential cross sections (left) and relative correction  $\delta$  (right), as functions of the transverse momentum of the top quark (up) and of the parton energy (down), at the LHC, with no additional cuts.

Contributions of all production channels are shown separately, as well as combined to the total correction.

At the LHC, the largest correction comes from the photon–gluon production channel at NLO. It has the same sign as the contribution to the  $gg$  fusion which is the dominant  $t\bar{t}$  production channel at the LHC. However, the contributions to  $q\bar{q}$  annihilation have opposite signs which leads to a reduction of the overall NLO QED cor-

rection. In total, the relative correction is about 1% and is slightly reduced if the cuts are applied.

At the Tevatron, the largest contributions to the total hadronic cross section come from the  $u\bar{u}$  subprocess. The photon–gluon subprocess yields the second largest contribution, but with opposite sign. In total, the relative correction can amount to 2.5%, including cuts.

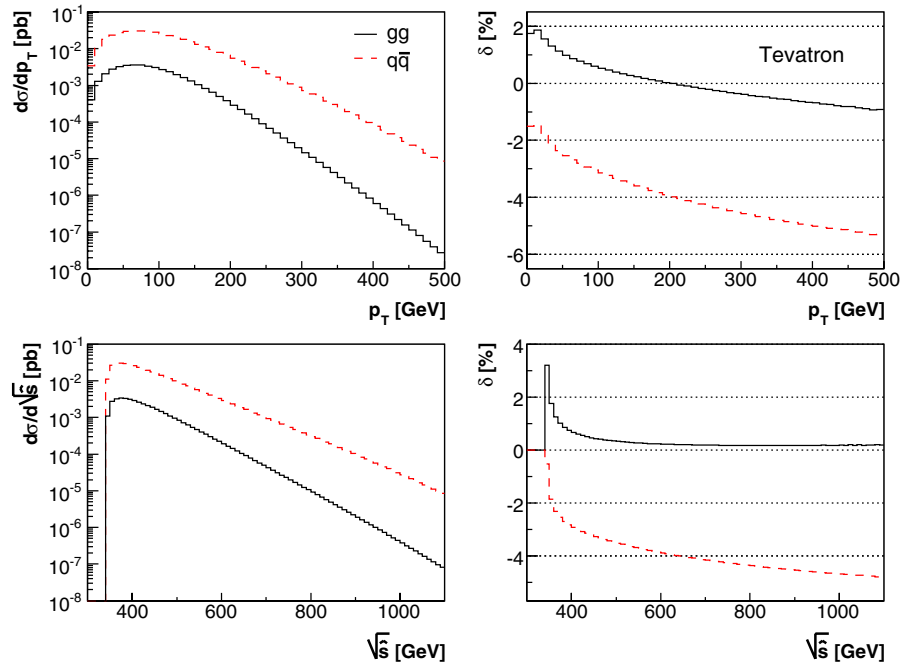


FIG. 10 (color online). Differential cross sections (left) and relative correction  $\delta$  (right), as functions of the transverse momentum of the top quark (up) and of the parton energy (down), at the Tevatron, with no additional cuts.

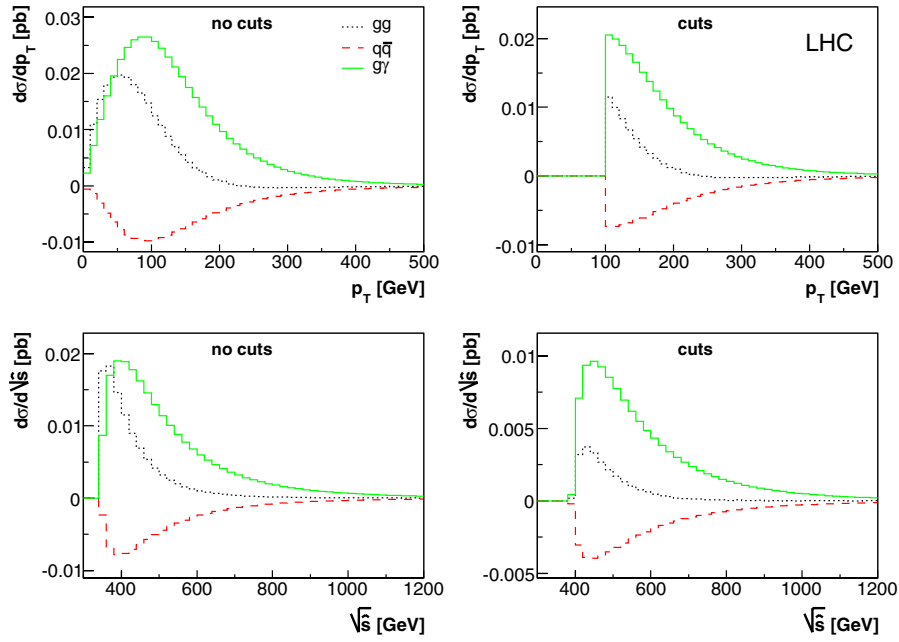


FIG. 11 (color online). NLO QED contributions from the  $gg$ ,  $q\bar{q}$ , and  $g\gamma$  channels at the LHC for the  $p_T$  and  $\sqrt{\hat{s}}$  distributions, including also cuts.

For illustration of the numerical impact of the NLO QED corrections on the distributions, we introduce the relative correction  $\delta$ , defined as

$$\delta = \frac{d\sigma_{\text{NLO}} - d\sigma_{\text{B}}}{d\sigma_{\text{B}}}, \quad (21)$$

with cross section at NLO,  $d\sigma_{\text{NLO}}$ , and the Born cross section  $d\sigma_{\text{B}}$ .

In Fig. 9 the  $p_T$  and  $\sqrt{\hat{s}}$  distributions are shown (left), as well as the relative QED corrections (right), for the  $gg$  and  $q\bar{q}$  parton channel at the LHC. The effect of the NLO QED corrections in the dominant  $gg$  fusion channel is rather small, less than 1% over most of the  $p_T$  range and also over most of the  $\sqrt{\hat{s}}$  range. Differently from the  $gg$  channel, the NLO contributions for  $q\bar{q}$  annihilation are negative over the whole  $p_T$  and  $\sqrt{\hat{s}}$  range, reaching the 5% level

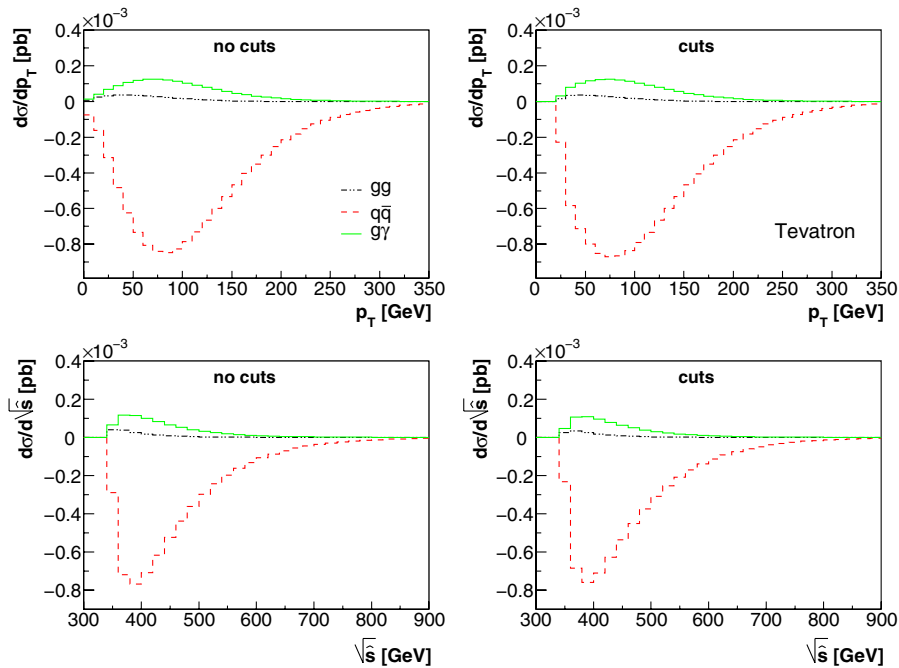


FIG. 12 (color online). NLO QED contributions from the  $gg$ ,  $q\bar{q}$ , and  $g\gamma$  channels at the Tevatron for the  $p_T$  and  $\sqrt{\hat{s}}$  distributions, including also cuts.



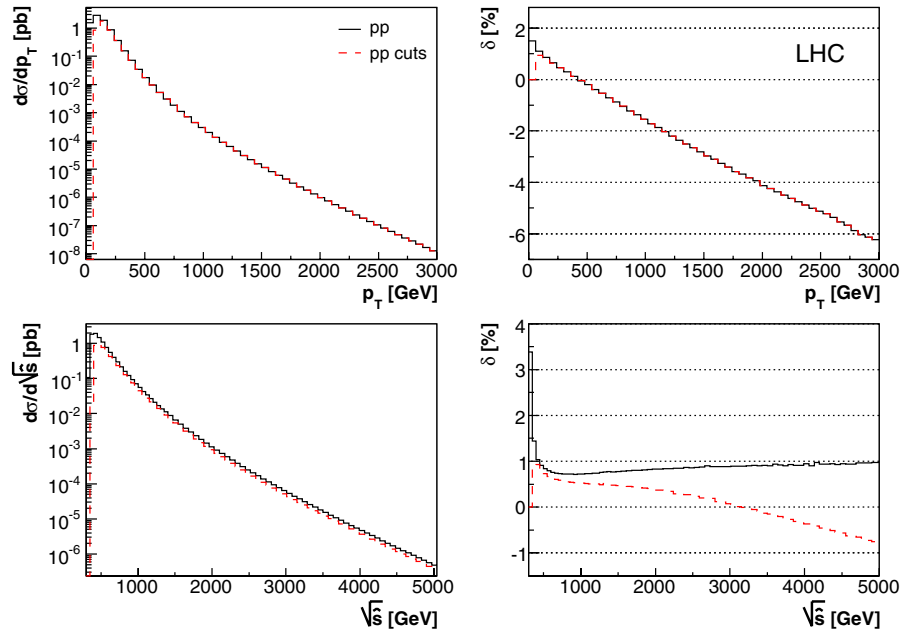


FIG. 13 (color online). Overall NLO QED effects in  $pp$  collisions at the LHC, for the  $p_T$  distribution (up) and the  $\sqrt{s}$  distribution (down), without and with application of cuts.

for  $p_T \geq 400$  GeV and  $\sqrt{s} \geq 1200$  GeV. They further grow in size with increasing  $p_T$  and  $\sqrt{s}$  and for very high  $p_T$  the  $q\bar{q}$  channel starts to dominate over the  $gg$  fusion.

In case of the Tevatron (Fig. 10), the  $q\bar{q}$  annihilation dominates over the  $gg$  fusion (left). The impact of  $\mathcal{O}(\alpha\alpha_s^2)$  corrections on both channels is similar to the LHC. Again, in the  $gg$  fusion, the relative correction  $\delta$  is smaller than 1% for most of the  $p_T$  and  $\sqrt{s}$  ranges, except for the low  $p_T$

and threshold regions where it reaches about 2% (upper right). In the  $q\bar{q}$  annihilation channel, the relative corrections are negative and at a few percent level already near the threshold. They grow further in size with increasing  $p_T$  and  $\sqrt{s}$ . The 5% level is reached for  $p_T \geq 350$  GeV and  $\sqrt{s} \geq 900$  GeV.

As previously discussed, also the photon-induced processes represent contributions of NLO in QED, owing to

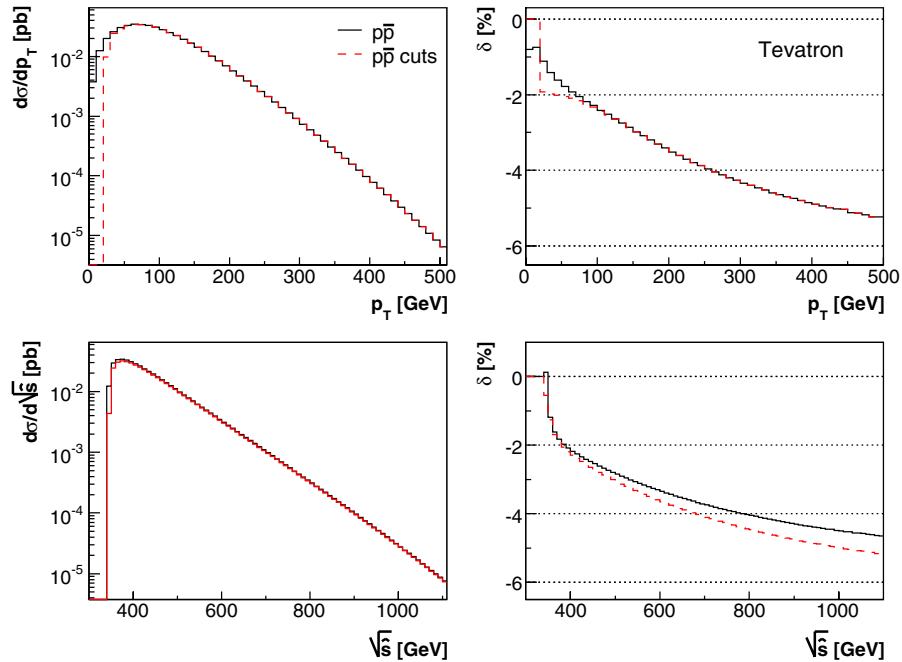


FIG. 14 (color online). Overall NLO QED effects in  $p\bar{p}$  collisions at the Tevatron, for the  $p_T$  distribution (up) and the  $\sqrt{s}$  distribution (down), without and with application of cuts.

higher order effects included in the PDFs. In Figs. 11 and 12, we show the photon–gluon contribution to  $t\bar{t}$  production, in comparison with the NLO terms in the  $gg$  and  $q\bar{q}$  channels. For the LHC (Fig. 11), the photon-induced contribution is larger than the corrections to both Born processes, a consequence of the fact that the combination of gluon and photon parton densities can become substantially large. Since  $g\gamma$  hadronic cross section is of the same sign as the NLO contributions to the  $gg$  fusion channel, its presence enhances the size of the overall NLO QED contributions.

The situation is different at the Tevatron (Fig. 12), where the  $q\bar{q}$  annihilation channel dominates. Still, the photon-induced contribution is larger in size than the NLO QED corrections to the  $gg$  fusion channel. However, as a consequence of opposite signs, these two tend to reduce the contribution from the  $q\bar{q}$  channel.

Finally, we show the combination of the partial results for all production subprocesses, including the photon–gluon channel, in Fig. 13 for the LHC and in Fig. 14 for the Tevatron. As a consequence of the dominant  $gg$  production channel at the LHC, the total NLO QED corrections in the  $\sqrt{s}$  distribution are positive and at the level of about 1%. After applying the cuts and in the  $p_T$  distribution the corrections become negative and tend to increase in size with  $p_T$  and  $\sqrt{s}$ . This is caused by the logarithmic final state radiation contribution which is not canceled by the virtual corrections in case of noninclusive quantities.

At the Tevatron, with the dominating  $q\bar{q}$  channels, the total NLO QED corrections have a larger impact owing to the subtleties of the QED–QCD interference, which is not present at the Born level. They are negative and in size of several percent, becoming larger with increasing  $p_T$  and  $\sqrt{s}$ , and are slightly enhanced by the application of cuts.

Further steps in improving the theoretical predictions would be to combine the QED/electroweak NLO contributions with the QCD corrections. Presently, uncertainties from QCD corrections and PDFs are estimated to be about 9% at NLO, and are reduced to about 4% at NNLO [15] (for the total cross section). The QED corrections are of the same magnitude as the NNLO QCD uncertainties. For the distributions, in particular, when the NLO QED corrections are combined with the residual EW corrections, the electroweak/QED higher order effects become comparable in size with the NLO QCD contributions.

## V. CONCLUSION

We have provided the last missing item for a complete EW one-loop calculation for  $t\bar{t}$  production at hadron colliders. The NLO QED contributions form, together with the nonphotonic EW contributions, the complete EW corrections to  $t\bar{t}$  production at the one-loop level. For consistency and IR-finiteness, interference terms between QED and QCD have to be taken into account, for both virtual and

real (bremsstrahlung) contributions. Moreover, a new class of photon-induced  $t\bar{t}$  production parton processes occurs, which for the LHC yields larger effects than the corrections to  $q\bar{q}$  annihilation and  $gg$  fusion. In size, the NLO QED contributions can reach the level of 5%. When combined with the rest of the EW corrections, the effects can become significantly large to find consideration for precision studies.

## APPENDIX: PHOTON/GLUON BREMSSTRAHLUNG

In the phase space slicing approach the phase space is divided into a region where the integrand is finite and into regions where the singularities occur. In the nonsingular case the integration is performed numerically whereas in the singular regions the integration is carried out analytically in the approximation that the photon or photonlike gluon is soft and/or collinear to a charged fermion.

We separate the soft and collinear part of the singular regions by introducing two cutoff parameters  $\Delta E$  and  $\Delta\theta$ . In the soft part the photon/gluon energy  $k^0$  satisfies the condition  $k^0 < \Delta E \ll \sqrt{s}$ , while in the collinear part we have  $k^0 > \Delta E$  and  $\theta_{\gamma f} < \Delta\theta$ , where  $\theta_{\gamma f}$  is the angle between the photon and a charged fermion.

In both regions the squared matrix elements for the radiative process factorize into the lowest-order matrix elements and universal factors containing the singularities. Thus, we can decompose the real corrections into

$$d\hat{\sigma}_{\text{real}}^a = d\hat{\sigma}_{\text{soft}}^a + d\hat{\sigma}_{\text{coll}}^a + d\hat{\sigma}_{\text{finite}}^a, \quad (\text{A1})$$

where  $a = q\bar{q}, gg$ . The collinear contribution is zero in  $gg$  fusion, and in the case of  $q\bar{q}$  annihilation only initial state radiation contributes since there are no mass singularities related to the final state bremsstrahlung.

The soft part is combined with IR and mass-singular virtual corrections to cancel the IR singularities proportional to  $\ln(\lambda)$  and the mass singularities of double logarithms  $\ln^2(m_q)$ . The single logarithms  $\ln(m_q)$  are not compensated in the sum of virtual and real corrections and have to be handled by means of factorization. Single virtual and real contributions are dependent on the cutoff parameters  $\Delta E$  and  $\Delta\theta$ . However, the dependence has to cancel in the combination (A1).

The soft photon/gluon bremsstrahlung cross sections can be factorized into soft factors and the Born cross sections,

$$\begin{aligned} d\hat{\sigma}_{\text{soft}}^{q\bar{q}} &= -\frac{\alpha}{\pi} d\hat{\sigma}_{\text{Born}}^{q\bar{q}} \cdot (C_q + C_t + C_{qt}), \\ d\hat{\sigma}_{\text{soft}}^{gg} &= -\frac{\alpha}{\pi} d\hat{\sigma}_{\text{Born}}^{gg} \cdot C_t, \end{aligned} \quad (\text{A2})$$

with  $C_q, C_t, C_{qt}$  referring to initial state radiation, final state radiation, and initial–final state radiation interference, respectively,

$$\begin{aligned}
C_q &= Q_q^2 \left[ 2 \ln\left(\frac{2\Delta E}{\lambda}\right) + 2 \ln\left(\frac{2\Delta E}{\lambda}\right) \ln\left(\frac{m_q^2}{\hat{s}}\right) + \frac{1}{2} \ln^2\left(\frac{m_q^2}{\hat{s}}\right) + \ln\left(\frac{m_q^2}{\hat{s}}\right) + \frac{\pi^2}{3} \right], \\
C_t &= Q_t^2 \left[ 2 \ln\left(\frac{2\Delta E}{\lambda}\right) + \frac{1}{\beta} \ln\left(\frac{1-\beta}{1+\beta}\right) + \frac{\hat{s}-2m_t^2}{\hat{s}\beta} \left\{ 2 \ln\left(\frac{2\Delta E}{\lambda}\right) \ln\left(\frac{1-\beta}{1+\beta}\right) + \frac{1}{2} \ln^2\left(\frac{1-\beta}{1+\beta}\right) + 2 \text{Li}_2\left(\frac{2\beta}{1+\beta}\right) \right\} \right], \\
C_{qt} &= 2Q_q Q_t \cdot 3 \left[ 2 \ln\left(\frac{2\Delta E}{\lambda}\right) \ln\left(\frac{m_t^2 - \hat{u}}{m_t^2 - \hat{t}}\right) + \text{Li}_2\left(1 - \frac{\hat{s}(1+\beta)}{2(m_t^2 - \hat{t})}\right) + \text{Li}_2\left(1 - \frac{\hat{s}(1-\beta)}{2(m_t^2 - \hat{t})}\right) - \text{Li}_2\left(1 - \frac{\hat{s}(1+\beta)}{2(m_t^2 - \hat{u})}\right) \right. \\
&\quad \left. - \text{Li}_2\left(1 - \frac{\hat{s}(1-\beta)}{2(m_t^2 - \hat{u})}\right) \right], \tag{A3}
\end{aligned}$$

with  $\beta = \sqrt{1 - 4m_t^2/\hat{s}}$ . The additional factor of 3 in the interference term comes from the gluon radiation contribution.

The collinear part of initial state radiation arises only for photons from the  $q\bar{q}$  annihilation channel, and can be expressed as follows (see e.g. [45]):

$$d\hat{\sigma}_{\text{coll}}^{q\bar{q}}(\hat{s}) = \frac{Q_q^2 \alpha}{\pi} \int_0^{1-2\Delta E/\sqrt{\hat{s}}} dz d\hat{\sigma}_{\text{Born}}^a(z\hat{s}) \left\{ \left[ \ln\left(\frac{\Delta\theta^2 \hat{s}}{4m_q^2}\right) - 1 \right] P_{qq}(z) + (1-z) \right\}, \tag{A4}$$

with the splitting function

$$P_{qq}(z) = \frac{1+z^2}{1-z}. \tag{A5}$$

- 
- [1] F. Abe *et al.* (CDF Collaboration), Phys. Rev. Lett. **74**, 2626 (1995).  
[2] S. Abachi *et al.* (D0 Collaboration), Phys. Rev. Lett. **74**, 2632 (1995).  
[3] J. Alcaraz *et al.* (ALEPH, DELPHI, L3, OPAL, and LEP Electroweak Working Group Collaborations [LEP Collaborations]), arXiv:hep-ex/0612034.  
[4] M. Glück, J. F. Owens, and E. Reya, Phys. Rev. D **17**, 2324 (1978). B. L. Combridge, Nucl. Phys. **B151**, 429 (1979); J. Babcock, D. W. Sivers, and S. Wolfram, Phys. Rev. D **18**, 162 (1978); K. Hagiwara and T. Yoshino, Phys. Lett. B **80**, 282 (1979); L. M. Jones and H. W. Wyld, Jr., Phys. Rev. D **17**, 2332 (1978); H. M. Georgi, S. L. Glashow, M. E. Machacek, and D. V. Nanopoulos, Ann. Phys. (N.Y.) **114**, 273 (1978).  
[5] U. Baur, E. W. N. Glover, and A. D. Martin, Phys. Lett. B **232**, 519 (1989).  
[6] P. Nason, S. Dawson, and R. K. Ellis, Nucl. Phys. **B303**, 607 (1988); **B327**, 49 (1989).  
[7] W. Beenakker, H. Kuijff, W. L. van Neerven, and J. Smith, Phys. Rev. D **40**, 54 (1989); W. Beenakker, W. L. van Neerven, R. Meng, G. A. Schuler, and J. Smith, Nucl. Phys. **B351**, 507 (1991).  
[8] V. S. Fadin and V. A. Khoze, JETP Lett. **46**, 525 (1987); V. S. Fadin, V. A. Khoze, and T. Sjöstrand, Z. Phys. C **48**, 613 (1990).  
[9] E. L. Berger and H. Contopanagos, Phys. Rev. D **54**, 3085 (1996); E. L. Berger and H. Contopanagos, Phys. Rev. D **57**, 253 (1998).  
[10] S. Catani, M. L. Mangano, P. Nason, and L. Trentadue, Phys. Lett. B **378**, 329 (1996). Nucl. Phys. **B478**, 273 (1996).  
[11] N. Kidonakis and J. Smith, Phys. Rev. D **51**, 6092 (1995).  
[12] E. Laenen, J. Smith, and W. L. van Neerven, Nucl. Phys. **B369**, 543 (1992); E. Laenen, J. Smith, and W. L. van Neerven, Phys. Lett. B **321**, 254 (1994).  
[13] R. Bonciani, S. Catani, M. L. Mangano, and P. Nason, Nucl. Phys. **B529**, 424 (1998).  
[14] M. Cacciari, S. Frixione, M. L. Mangano, P. Nason, and G. Ridolfi, J. High Energy Phys. **04** (2004) 068.  
[15] N. Kidonakis and R. Vogt, Phys. Rev. D **68**, 114014 (2003).  
[16] N. Kidonakis, Phys. Rev. D **73**, 034001 (2006).  
[17] W. Beenakker, A. Denner, W. Hollik, R. Mertig, T. Sack, and D. Wackerroth, Nucl. Phys. **B411**, 343 (1994).  
[18] C. Kao, G. A. Ladinsky, and C. P. Yuan, Int. J. Mod. Phys. A **12**, 1341 (1997).  
[19] J. H. Kühn, A. Scharf, and P. Uwer, Eur. Phys. J. C **45**, 139 (2006).  
[20] S. Moretti, M. R. Nolten, and D. A. Ross, Phys. Lett. B **639**, 513 (2006).  
[21] W. Bernreuther, M. Fuecker, and Z.-G. Si, Phys. Rev. D **74**, 113005 (2006).  
[22] J. H. Kühn, A. Scharf, and P. Uwer, arXiv:hep-ph/0610335.  
[23] A. Stange and S. Willenbrock, Phys. Rev. D **48**, 2054 (1993).  
[24] H.-Y. Zhou, C.-S. Li, and Y.-P. Kuang, Phys. Rev. D **55**, 4412 (1997).  
[25] S. Alam, K. Hagiwara, S. Matsumoto, K. Hagiwara, and S. Matsumoto, Phys. Rev. D **55**, 1307 (1997); Z. Sullivan, Phys. Rev. D **56**, 451 (1997); C.-S. Li, H.-Y. Zhou, Y.-L. Zhu, and J.-M. Yang, Phys. Lett. B **379**, 135 (1996); C.-S. Li, B.-Q. Hu, J.-M. Yang, and C.-G. Hu, Phys. Rev. D **52**,

- 5014 (1995).
- [26] J. Kim, J. L. Lopez, D. V. Nanopoulos, and R. Rangarajan, Phys. Rev. D **54**, 4364 (1996).
- [27] H.-Y. Zhou and C.-S. Li, Phys. Rev. D **55**, 4421 (1997).
- [28] S. Berge, W. Hollik, W. M. Möhle, and D. Wackerroth, Phys. Rev. D **76**, 034016 (2007).
- [29] W. Hollik, W. M. Möhle, and D. Wackerroth, Nucl. Phys. **B516**, 29 (1998).
- [30] C. Kao and D. Wackerroth, Phys. Rev. D **61**, 055009 (2000).
- [31] J. Küblbeck, M. Böhm, and A. Denner, Comput. Phys. Commun. **60**, 165 (1990); T. Hahn, Comput. Phys. Commun. **140**, 418 (2001); T. Hahn and C. Schappacher, Comput. Phys. Commun. **143**, 54 (2002).
- [32] T. Hahn and M. Perez-Victoria, Comput. Phys. Commun. **118**, 153 (1999).
- [33] T. Hahn, Acta Phys. Pol. B **30**, 3469 (1999); Nucl. Phys. B, Proc. Suppl. **89**, 231 (2000); T. Hahn and M. Rauch, Nucl. Phys. B, Proc. Suppl. **157**, 236 (2006).
- [34] G. 't Hooft and M. J. G. Veltman, Nucl. Phys. **B153**, 365 (1979).
- [35] G. Passarino and M. J. G. Veltman, Nucl. Phys. **B160**, 151 (1979).
- [36] W. Beenakker and A. Denner, Nucl. Phys. **B338**, 349 (1990).
- [37] A. Denner, U. Nierste, and R. Scharf, Nucl. Phys. **B367**, 637 (1991).
- [38] W. Beenakker, S. C. van der Marck, and W. Hollik, Nucl. Phys. **B365**, 24 (1991).
- [39] F. Bloch and A. Nordsieck, Phys. Rev. **52**, 54 (1937).
- [40] S. Dittmaier, Nucl. Phys. **B565**, 69 (2000).
- [41] S. Catani and M. H. Seymour, Phys. Lett. B **378**, 287 (1996); Nucl. Phys. **B485**, 291 (1997).
- [42] A. D. Martin, R. G. Roberts, W. J. Stirling, and R. S. Thorne, Eur. Phys. J. C **39**, 155 (2005).
- [43] U. Baur, S. Keller, and D. Wackerroth, Phys. Rev. D **59**, 013002 (1998).
- [44] K. P. O. Diener, S. Dittmaier, and W. Hollik, Phys. Rev. D **72**, 093002 (2005).
- [45] S. Dittmaier and M. Krämer, Phys. Rev. D **65**, 073007 (2002).